

Supporting Information

Ligand effect on Ru-centered species toward methane activation

*Mengdi Guo,^{ab} Xiaonan Wu,^{*c} Hechen Wu^d and Xiaoyan Sun^{*ab}*

^a Qingdao Institute of Bioenergy and Bioprocess Technology, Chinese Academy of Sciences, 266101 Qingdao (P. R. China).

^b Shandong Energy Institute, 266101 Qingdao (P. R. China).

^c East China Normal University, 200241 Shanghai (P. R. China)

^d Fudan University, 200240 Shanghai (P. R. China).

Xiaonan Wu*: E-mail: xnwu@chem.ecnu.edu.cn

Xiaoyan Sun*: E-mail: sunxy@qibebt.ac.cn

Contents

1. Experimental and theoretical results

Fig. S1 (A) Mass spectra of $\text{Ru}_3(\text{CO})_{12}$ dissolved in CH_3CN without and with source fragmentation. (B) Collision reduced dissociation process of $[\text{RuCH}(\text{CNH})_2(\text{CH}_3\text{CN})_2\text{CO}]^+$. (C) A possible model of the geometry of $[\text{RuCH}(\text{CNH})_2(\text{CH}_3\text{CN})_2\text{CO}]^+$. (Page S3)

Fig. S2 Reactions of $[\text{RuCH}]^+$ and $[\text{RuCHCNH}]^+$ with CD_4 . (Page S4)

Fig. S3 Reactions of monoisotopic $[\text{RuCH}]^+$ with CH_4 . (Page S4)

Fig. S4 Reactions of monoisotopic $[\text{RuCHCNH}]^+$ with CH_4 . (Page S5)

Fig. S5 Reaction of $[\text{RuCHCH}_2]^+$ and $[\text{RuCHCNHCH}_2]^+$ with CH_4 and CD_4 . (Page S6)

Fig. S6 Reaction of monoisotopic $[\text{RuCHCNHCH}_2]^+$ with CH_4 . (Page S6)

Fig. S7 Collision induced dissociation of products $[\text{RuCHCH}_2]^+$ and $[\text{RuCDCD}_2]^+$. (Page S7)

Fig. S8 Collision induced dissociation of products $[\text{RuCHCNHCH}_2]^+$ and $[\text{RuCHCNHCD}_2]^+$. (Page S7)

Fig. S9 Collision induced dissociation of monoisotopic products $[\text{RuCHCNHCH}_2]^+$ and $[\text{RuCHCND}_2]^+$ / $[\text{RuCDCNHCD}_2]^+$. (Page S8)

Fig. S10 CID processes of monoisotopic $[\text{RuCHCNH}]^+$. (Page S8)

Fig. S11 Stable structures of $[\text{RuC}]^+$, $[\text{RuCH}]^+$, $[\text{RuCNH}]^+$ and $[\text{RuCHCNH}]^+$. (Page S9)

Fig. S12 PES toward the reactions of ^{12}C - ^{13}C exchange of $[\text{RuCH}]^+/\text{CH}_4$ (blue line) and $[\text{RuCHCNH}]^+/\text{CH}_4$ (red line). Calculations are carried out at PBE0/def2-QZVPP//PBE0/def2-TZVPP level. Energies are in kJ/mol. (Page S9)

Fig. S13 PES toward the reactions of $[\text{RuC}]^+$ (a), $[\text{RuCH}]^+$ (b), $[\text{RuCNH}]^+$ (c) and $[\text{RuCHCNH}]^+$ (d-e) with CH_4 . (Page S10)

Fig. S14 PES toward the reaction of $[\text{RuNCCH}_2]^+$ with CH_4 . (Page S11)

Fig. S15 PES toward the reaction of $[\text{RuNCCH}_2]^+$ with H_2O and structural transformation between $[\text{RuNCCH}_2]^+$ and $[\text{RuCHCNH}]^+$. (Page S12)

Fig. S16 PES toward the reactions of $[\text{RuC}]^+$ with CH_4 . (Page S13)

Fig. S17 PES for the reaction of $[\text{RuCH}]^+$ with CH_4 toward product P. (Page S14)

Fig. S18 PES for the reaction of $[\text{RuCH}]^+$ with CH_4 toward product P*. (Page S14)

Fig. S19 PES for the reaction of $[\text{RuCH}]^+$ with CH_4 toward product P**. (Page S15)

Fig. S20 PES toward the reactions of $[\text{RuCNH}]^+$ with CH_4 . (Page S15)

Fig. S21 PES for the reaction of $[\text{RuCHCNH}]^+$ with CH_4 toward product P1 and P2. (Page S16)

Fig. S22 PES for the reaction of $[\text{RuCHCNH}]^+$ with CH_4 toward product P2. (Page S18)

Fig. S23 PES for the reaction of $[\text{RuCHCNH}]^+$ with CH_4 toward product P^{**}. (Page S19)

Fig. S24 Charge and spin populations on the transferring hydrogen of H involved transition states of $[\text{RuCH}]^+$ and $[\text{RuCHCNH}]^+$. (Page S20)

Fig. S25 Composition and occupancy of HOMOs of (a) $[\text{RuL}]^+$ (R), (b) $[\text{RuL}]^+/\text{CH}_4$ (I1) and transition states involved in the (c) first and (d) second rounds of hydrogen transfer. (Page S20)

Fig. S26 HOMOs (bottom) and LUMOs (top) of $[\text{RuL}]^+$ and CH_4 . (Page S22)

Fig. S27 Natural bond orbital (NBO) analysis of $[\text{RuL}]^+/\text{CH}_4$. (Page S22)

2. References

Page S23

1. Experimental and theoretical results

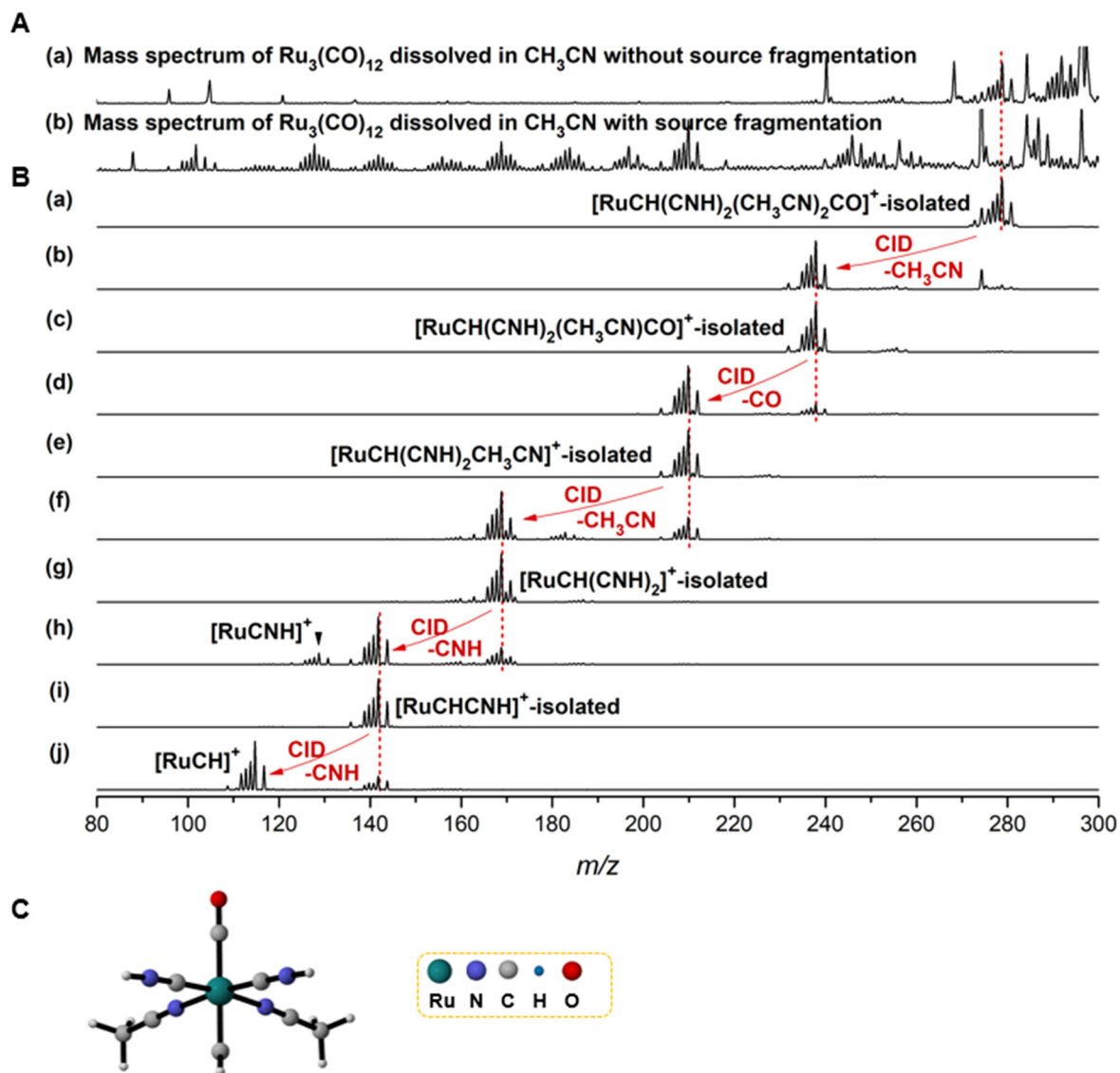


Fig. S1 (A) Mass spectra of $\text{Ru}_3(\text{CO})_{12}$ dissolved in CH_3CN without and with source fragmentation. (B) Collision reduced dissociation process of $[\text{RuCH}(\text{CNH})_2(\text{CH}_3\text{CN})_2\text{CO}]^+$. (C) A possible model of the geometry of $[\text{RuCH}(\text{CNH})_2(\text{CH}_3\text{CN})_2\text{CO}]^+$ built according to the CID process in Fig. S1B.

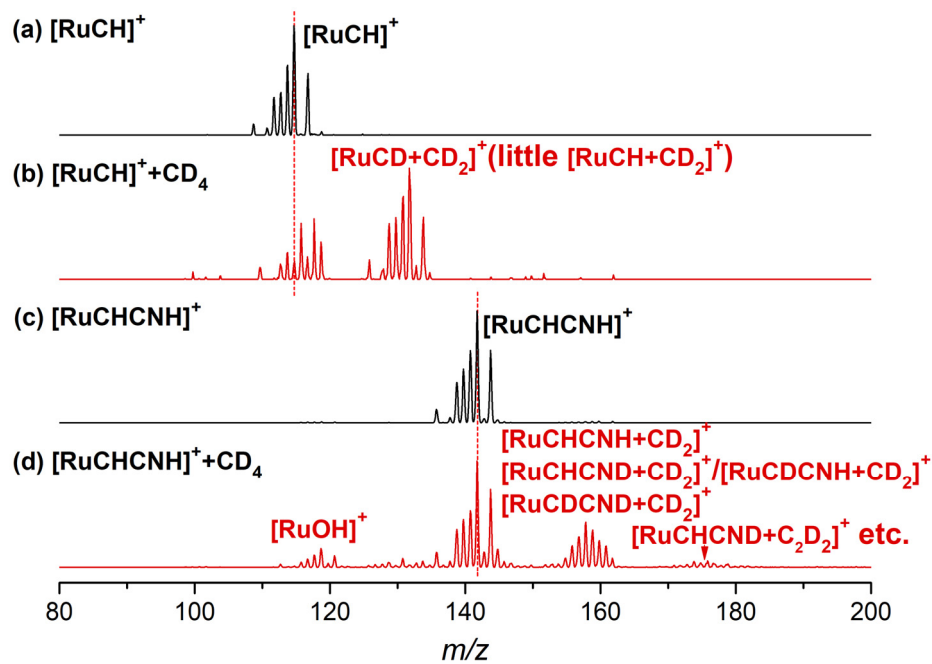


Fig. S2 Reactions of $[\text{RuCH}]^+$ and $[\text{RuCHCNH}]^+$ with CD_4 .

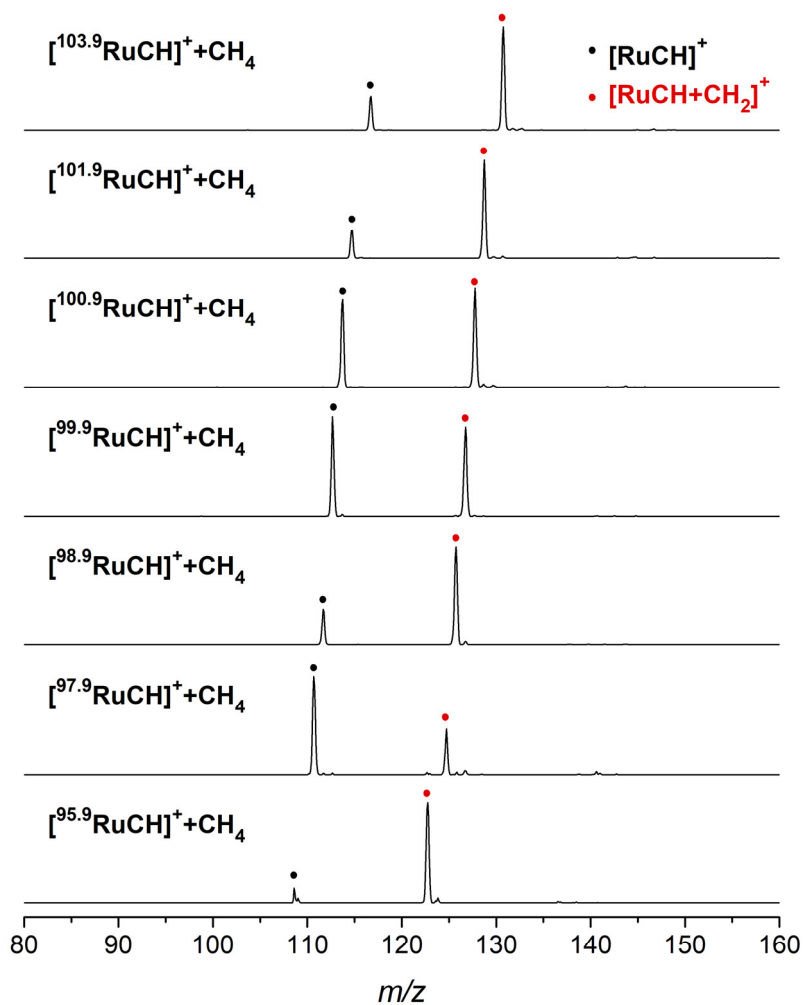


Fig. S3 Reactions of monoisotopic $[\text{RuCH}]^+$ with CH_4 .

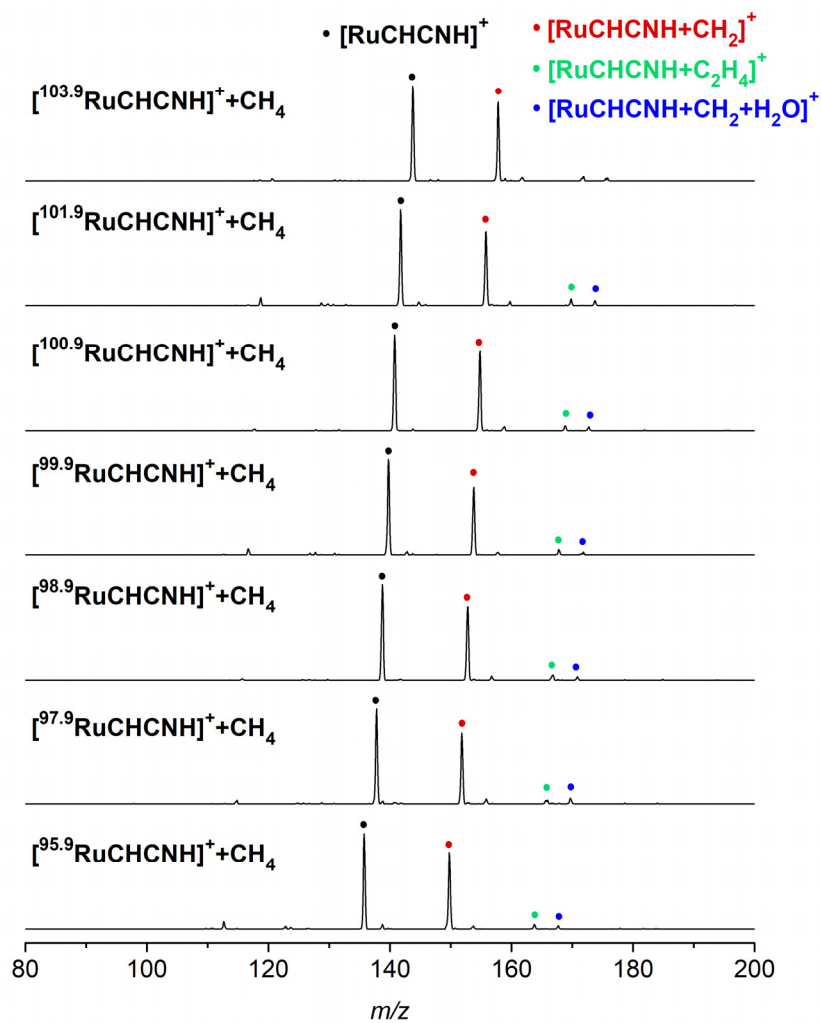


Fig. S4 Reactions of monoisotopic [RuCHCNH]⁺ with CH₄.

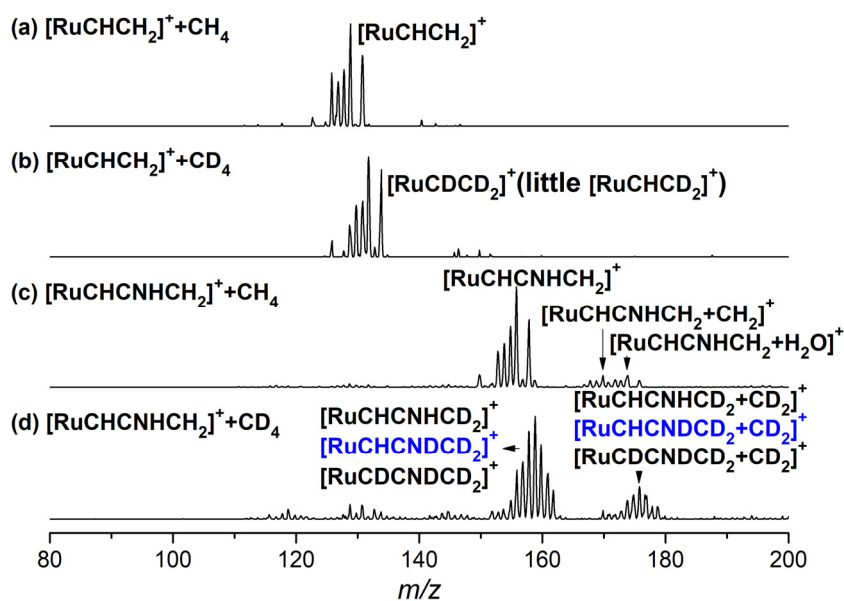


Fig. S5 Reaction of $[\text{RuCHCH}_2]^+$ and $[\text{RuCHCNHCH}_2]^+$ with CH_4 and CD_4 . Blue formulas could also be $[\text{RuCDCNHCD}_2]^+$ and $[\text{RuCDCNHCD}_2+\text{CD}_2]^+$.

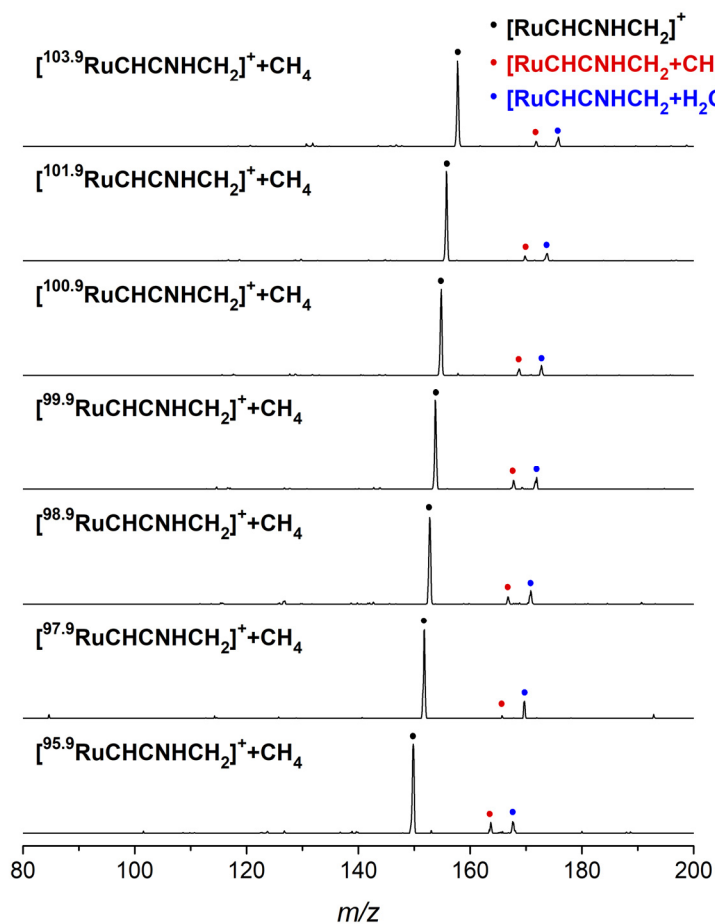


Fig. S6 Reaction of monoisotopic $[\text{RuCHCNHCH}_2]^+$ with CH_4 .

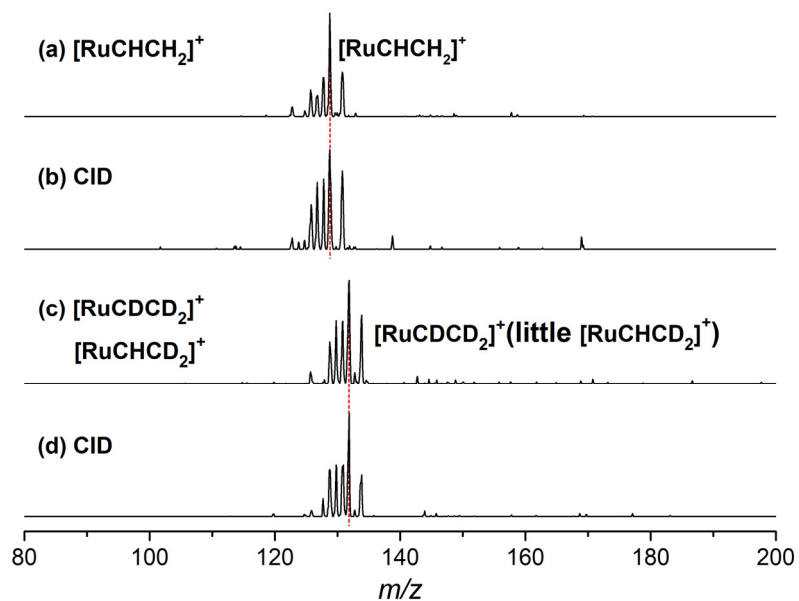


Fig. S7 Collision induced dissociation of products $[\text{RuCHCH}_2]^+$ and $[\text{RuCDCD}_2]^+$.

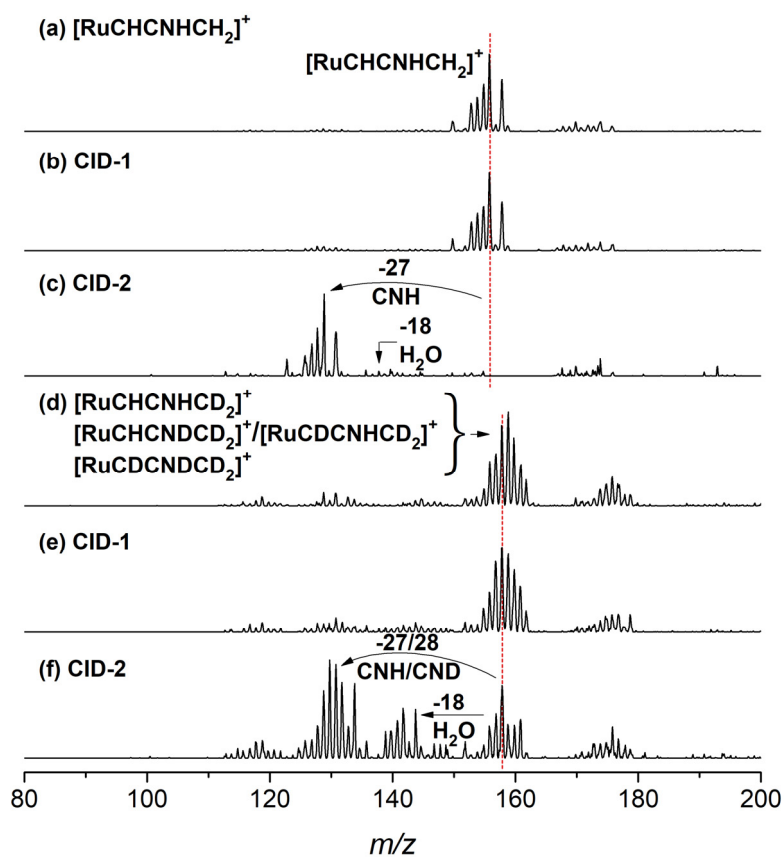


Fig. S8 Collision induced dissociation of products $[\text{RuCHCNHCH}_2]^+$ and $[\text{RuCHCNHCD}_2]^+$.

The intensity of water loss in collision induced dissociation of products $[\text{RuCHCNHCH}_2]^+$ on the mass spectra is affected by the background water and relatively intensity of CNH loss peak. Water loss is more clearly shown in Fig. S9.

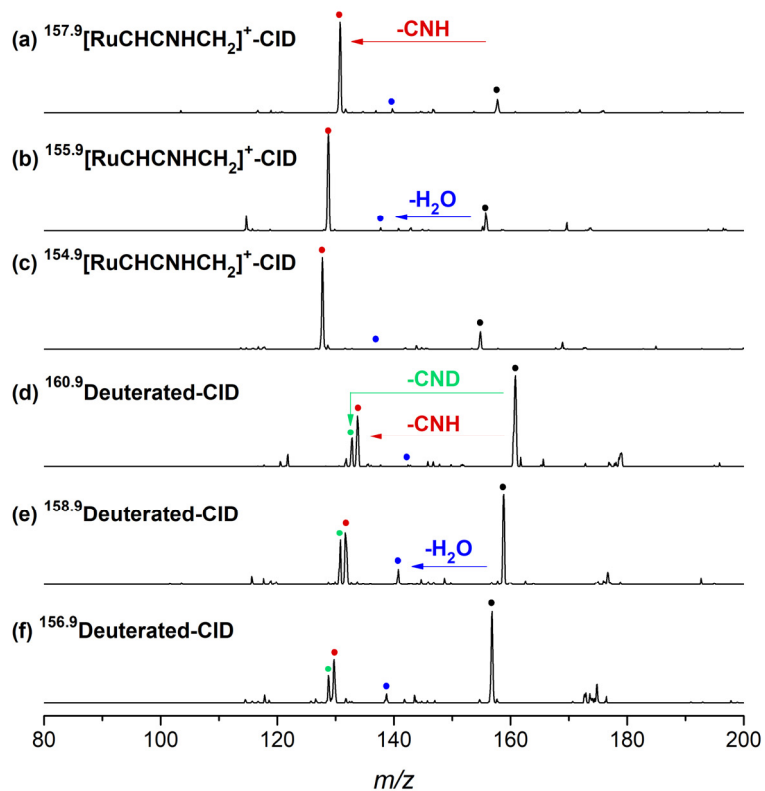


Fig. S9 Collision induced dissociation of monoisotopic products $[\text{RuCHCNHCH}_2]^+$ and $[\text{RuCHCNDCD}_2]^+ / [\text{RuCDCNHCD}_2]^+$.

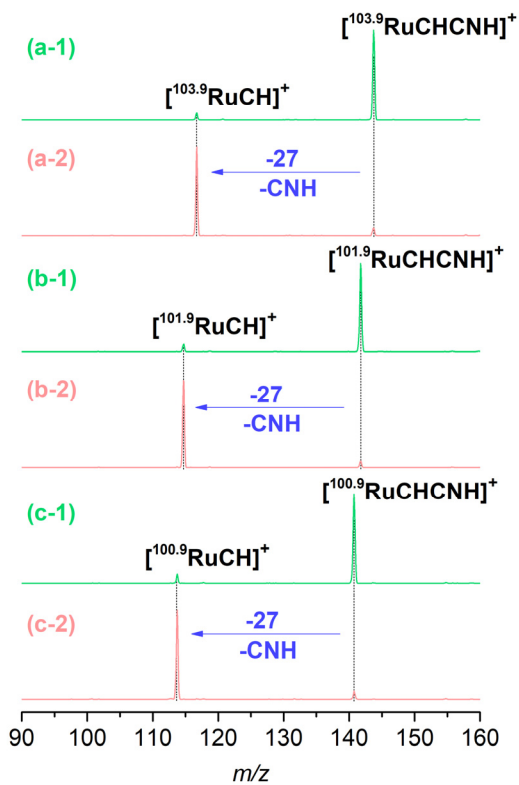


Fig. S10 CID of monoisotopic $[\text{RuCHCNH}]^+$ (green: low collision energy, pink: high collision energy).

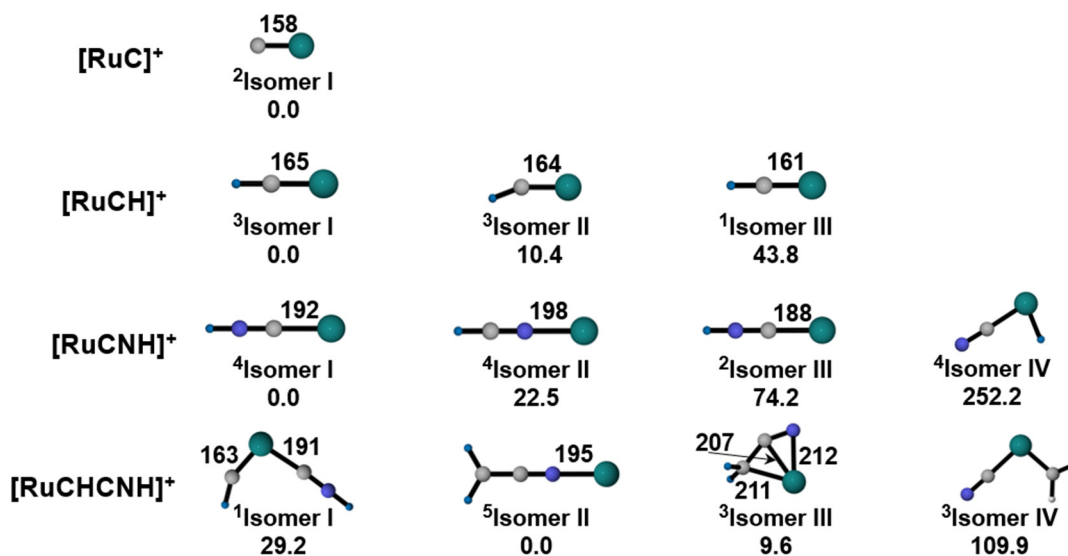


Fig. S11 Stable structures of [RuC]⁺, [RuCH]⁺, [RuCNH]⁺ and [RuCHCNH]⁺. Energies and bond length are in kJ/mol and pm.

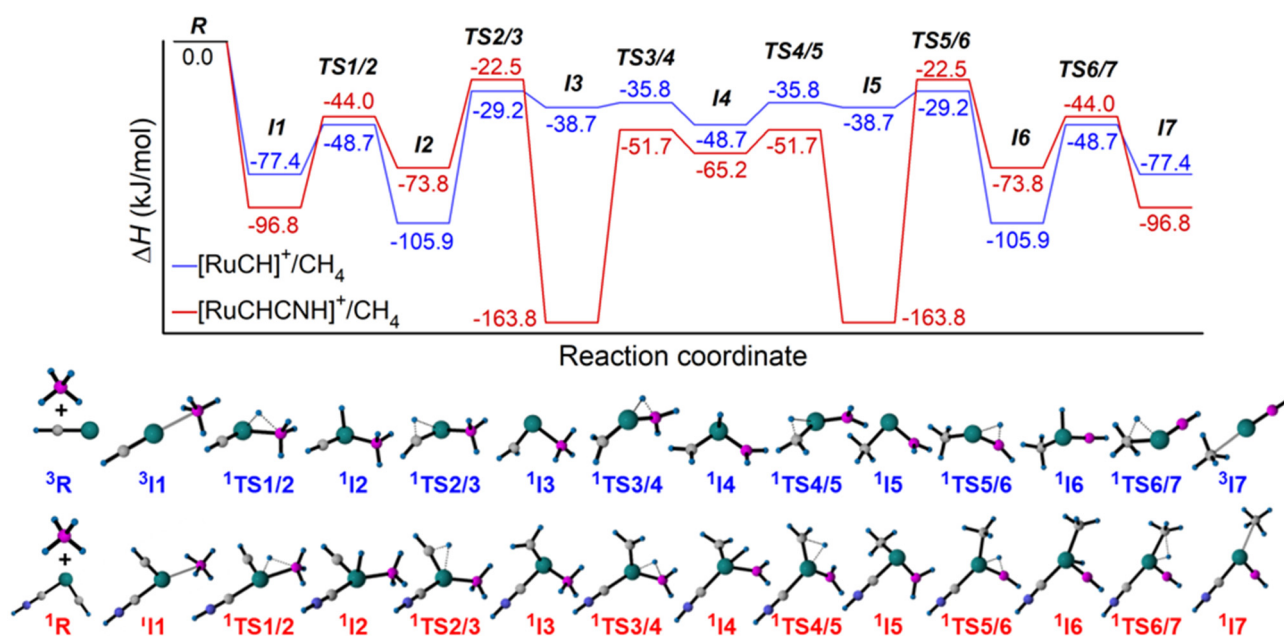


Fig. S12 PES toward the reactions of ¹²C-¹³C exchange of [RuCH]⁺/CH₄ (blue line) and [RuCHCNH]⁺/CH₄ (red line). Calculations are carried out at PBE0/def2-QZVPP//PBE0/def2-TZVPP level. Energies are in kJ/mol.

As shown in Fig. S12, ¹²C/¹³C exchange in [RuCH]⁺/CH₄ system is spontaneous and mild process, conforming the feasibility of ¹²C/¹³C exchange occurring before CH₄ activation without CID.

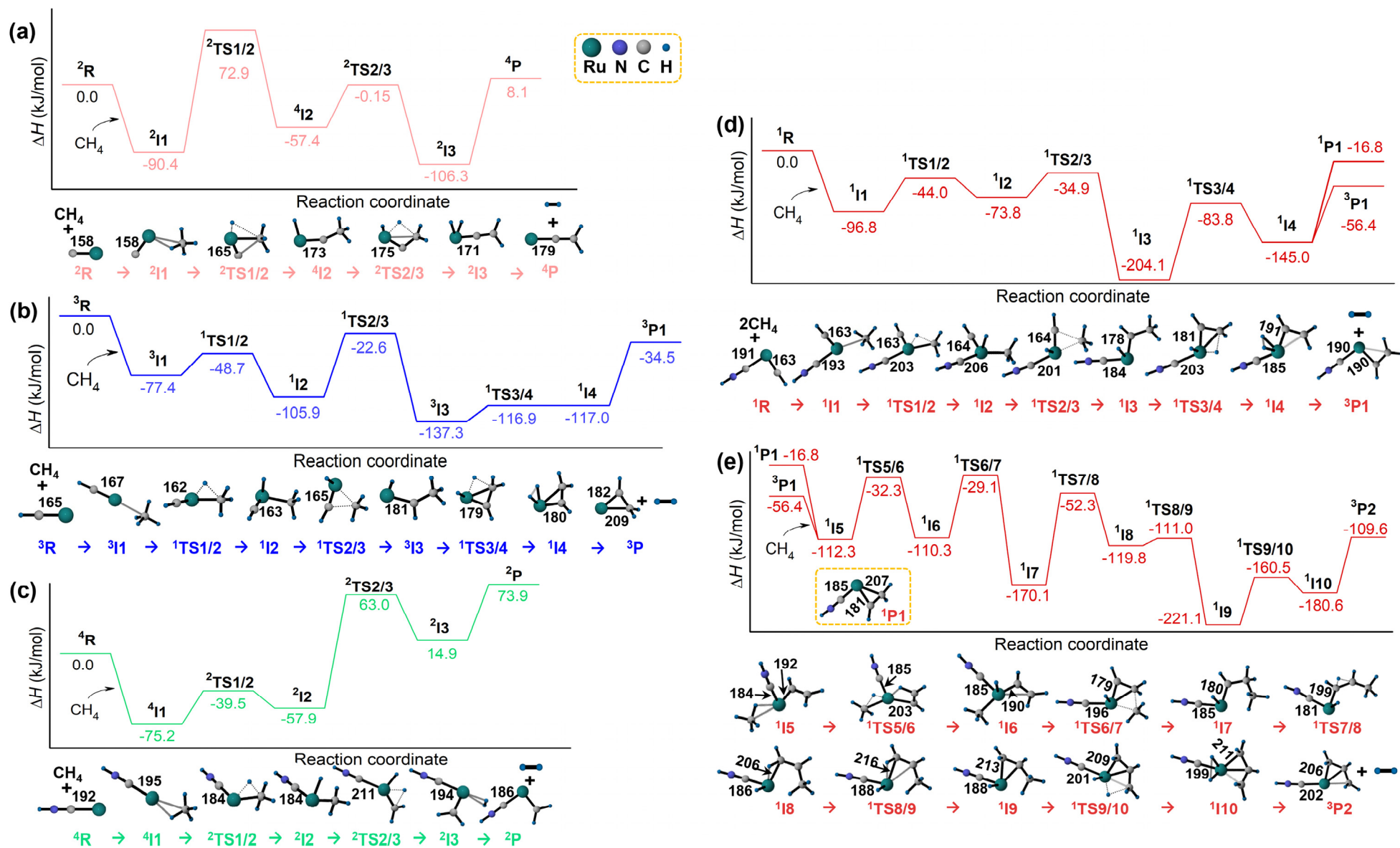


Fig. S13 PES toward the reactions of $[\text{RuC}]^+$ (a), $[\text{RuCH}]^+$ (b), $[\text{RuCNH}]^+$ (c) and $[\text{RuCHCNH}]^+$ (d-e) with CH_4 . Calculations are carried out at PBE0/def2-QZVPP//PBE0/def2-TZVPP level. Energies are in kJ/mol.

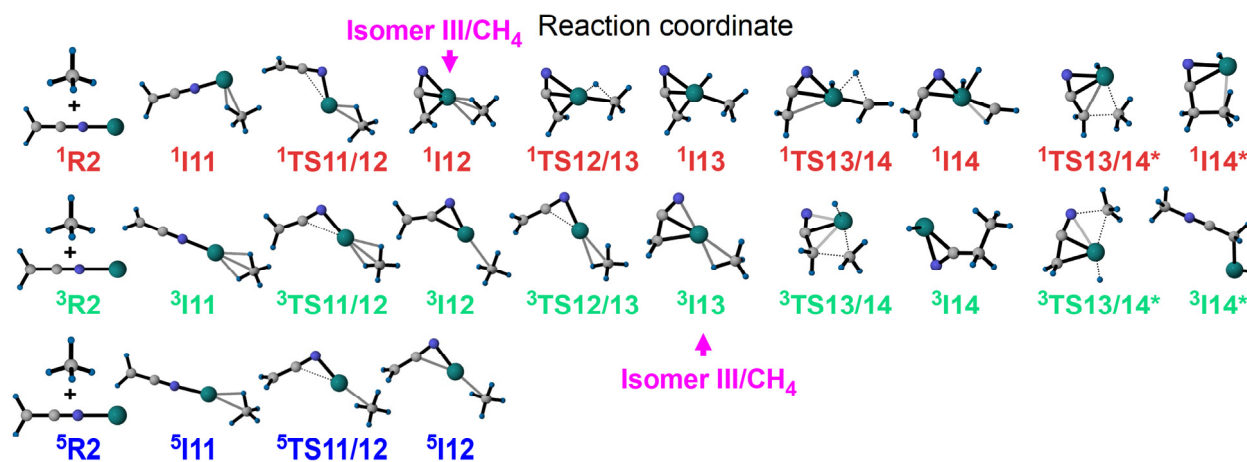
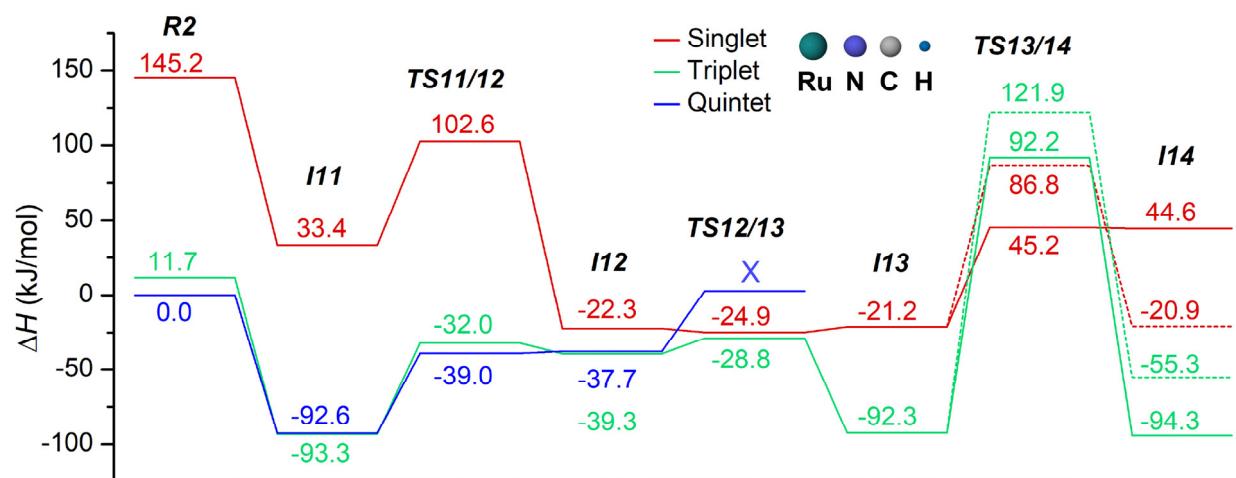


Fig. S14 PES toward the reaction of [RuNCCH₂]⁺ with CH₄. Energies are in kJ/mol.

The singlet transition state ¹TS12/13 is slightly lower in energy than ¹I12 and ¹I13 because of the the zero-point vibration energy (ZPE) correction.^[1] However, IRC calculations clearly demonstrate the link between ¹TS12/13 and ¹I13.

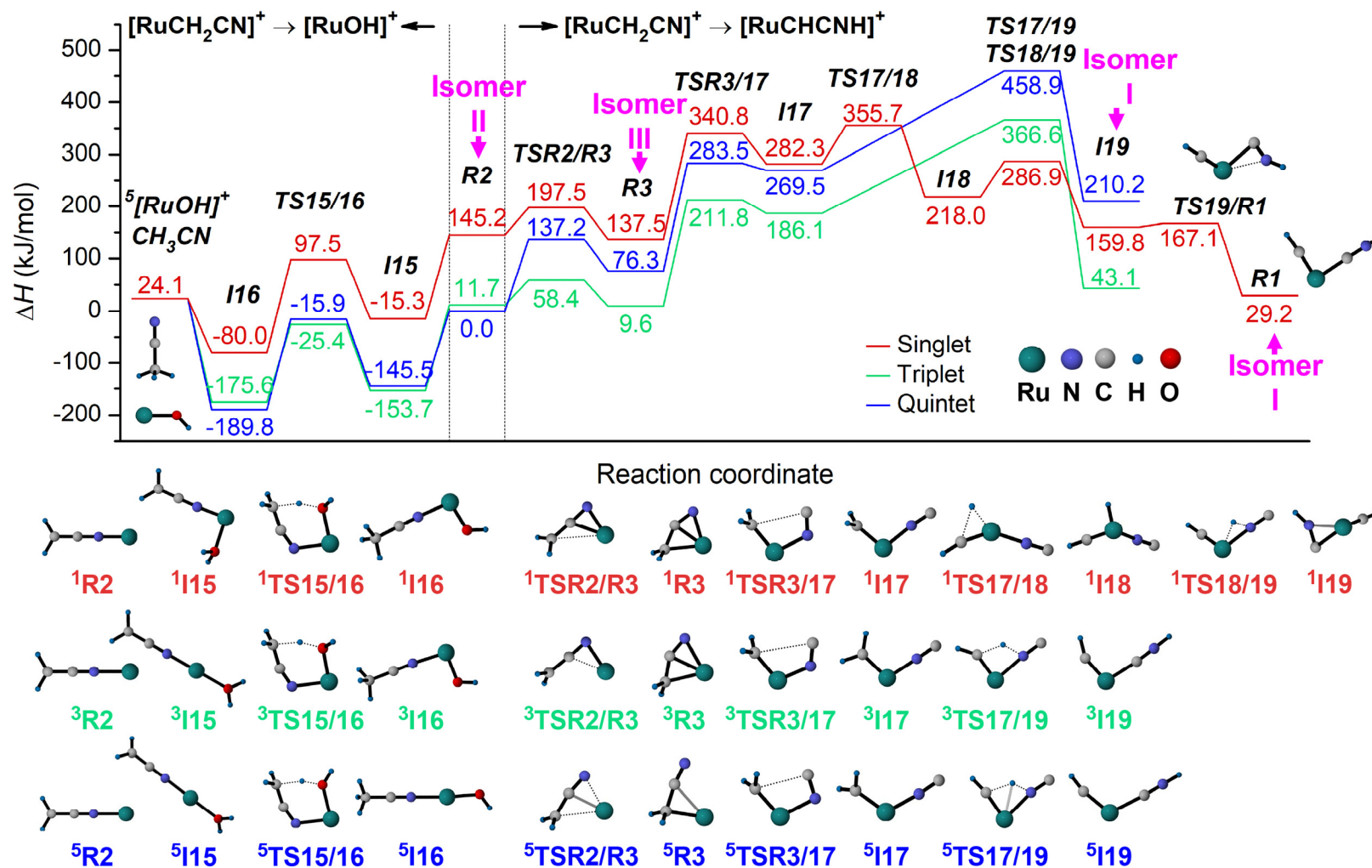


Fig. S15 PES toward the reaction of $[RuNCCH_2]^+$ with H_2O and structural transformation between $[RuNCCH_2]^+$ and $[RuCHCNH]^+$. Energies are in kJ/mol.

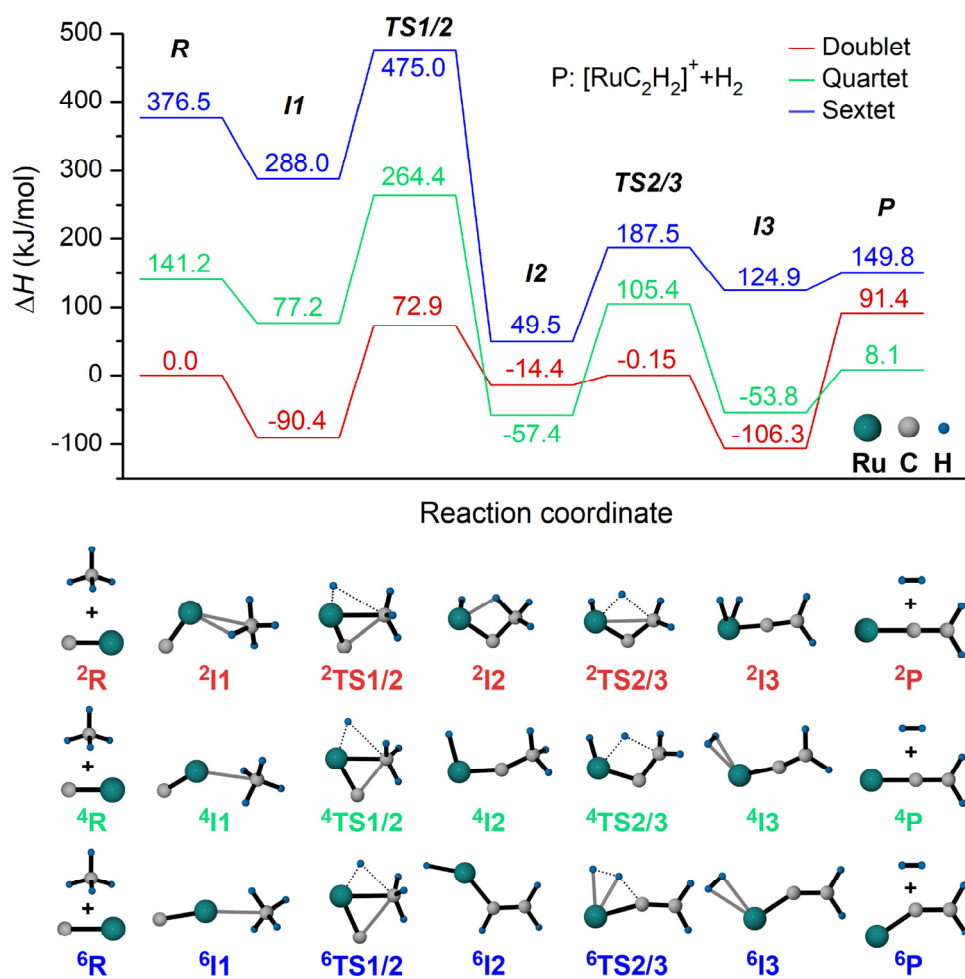


Fig. S16 PES toward the reaction of $[RuC]^+$ with CH_4 . Energies are in kJ/mol.

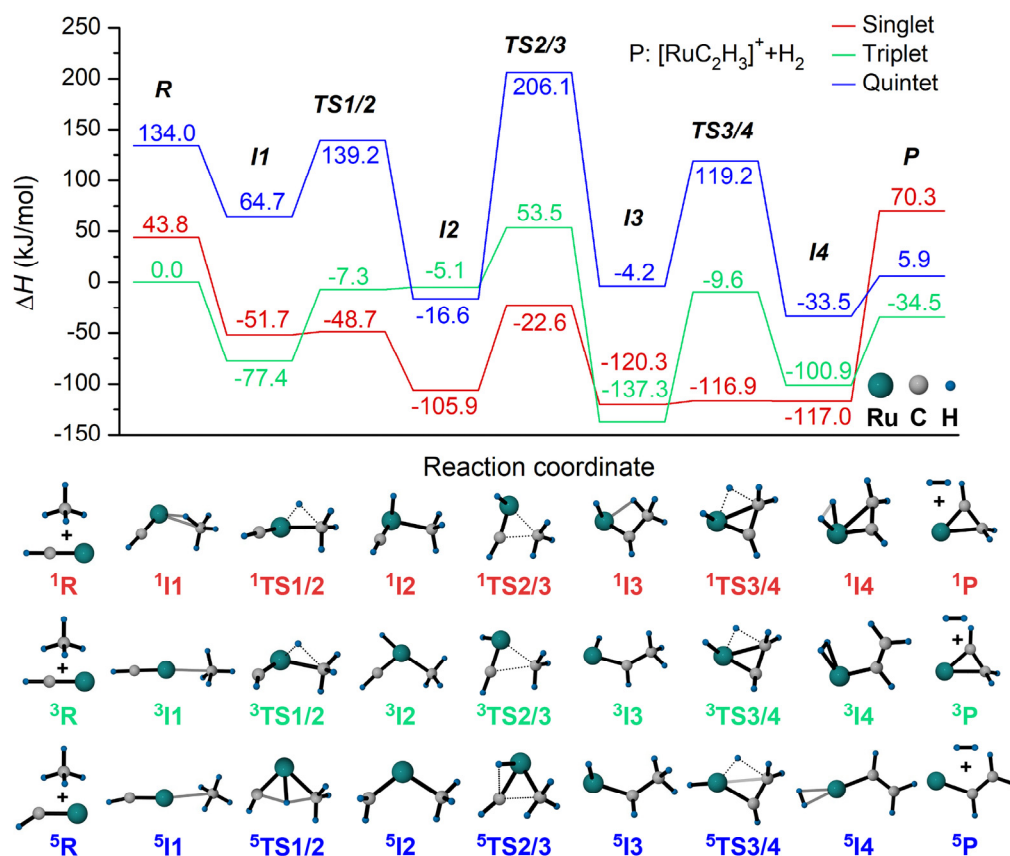


Fig. S17 PES for the reaction of $[\text{RuCH}]^+$ with CH_4 toward product P. Energies are in kJ/mol.

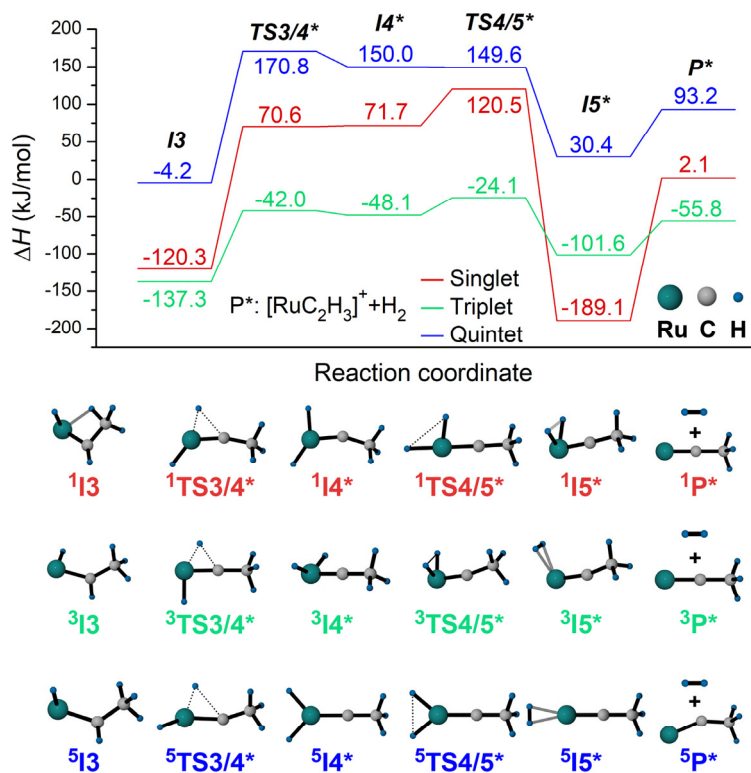


Fig. S18 PES for the reaction of $[\text{RuCH}]^+$ with CH_4 toward product P*. Energies are in kJ/mol.

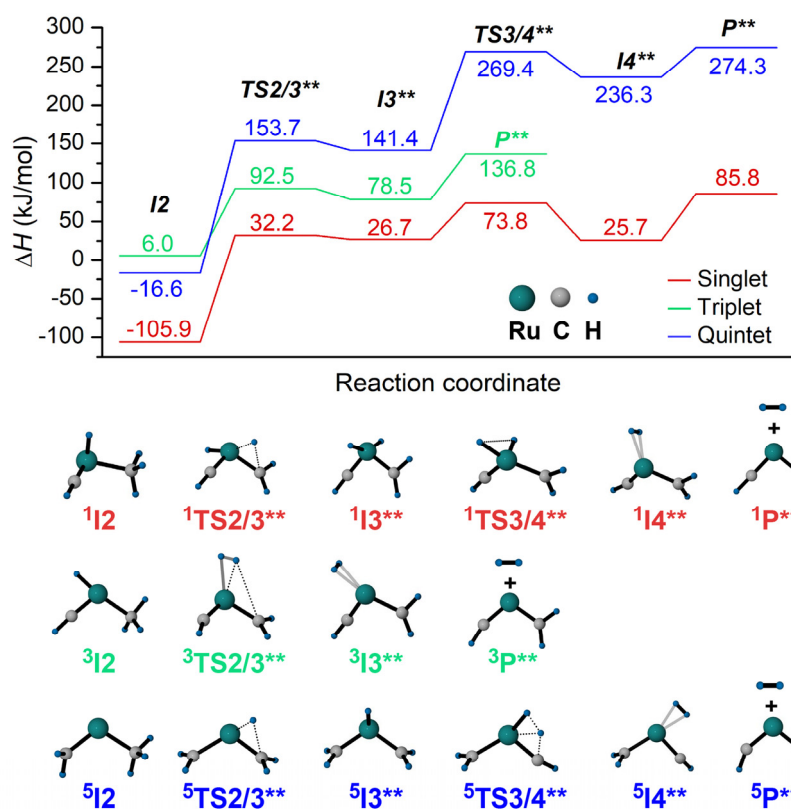


Fig. S19 PES for the reaction of $[\text{RuCH}]^+$ with CH_4 toward product P^{**} . Energies are in kJ/mol.

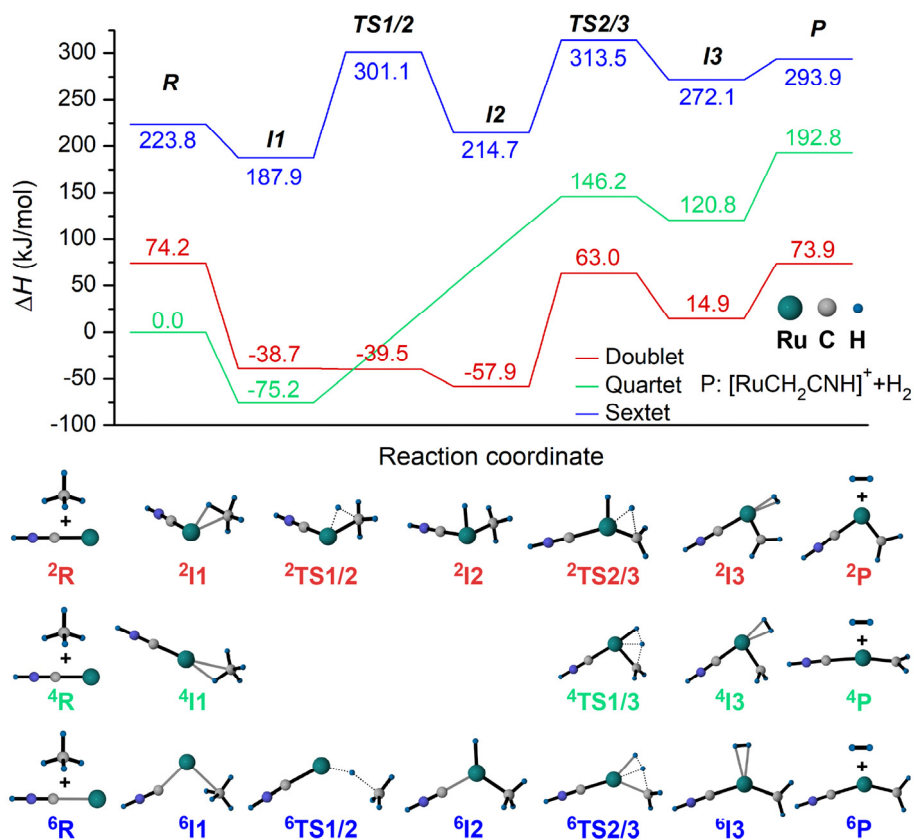


Fig. S20 PES for the reaction of $[\text{RuCNH}]^+$ with CH_4 . Energies are in kJ/mol.

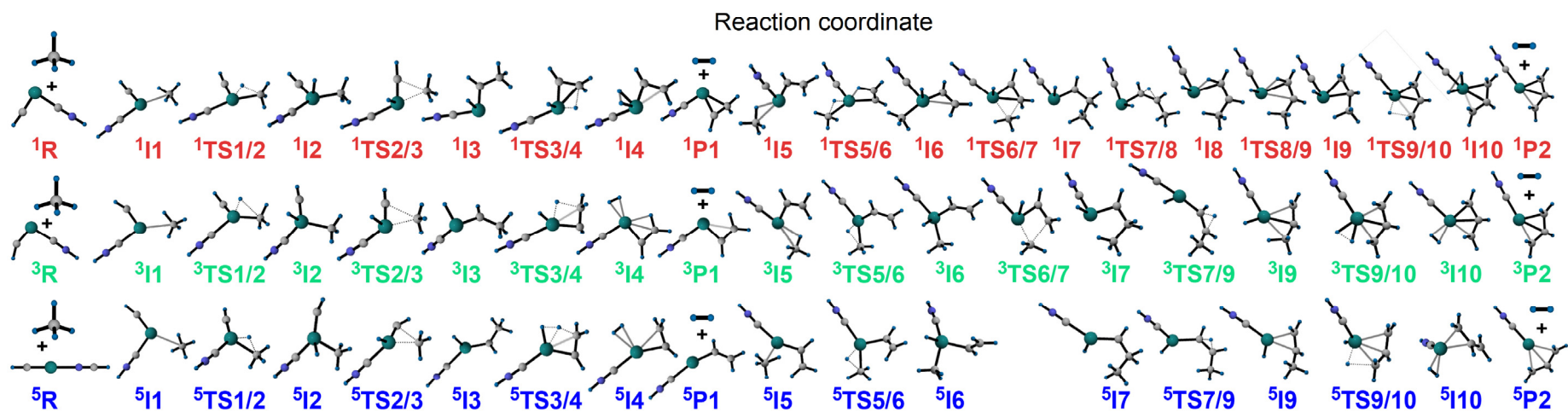
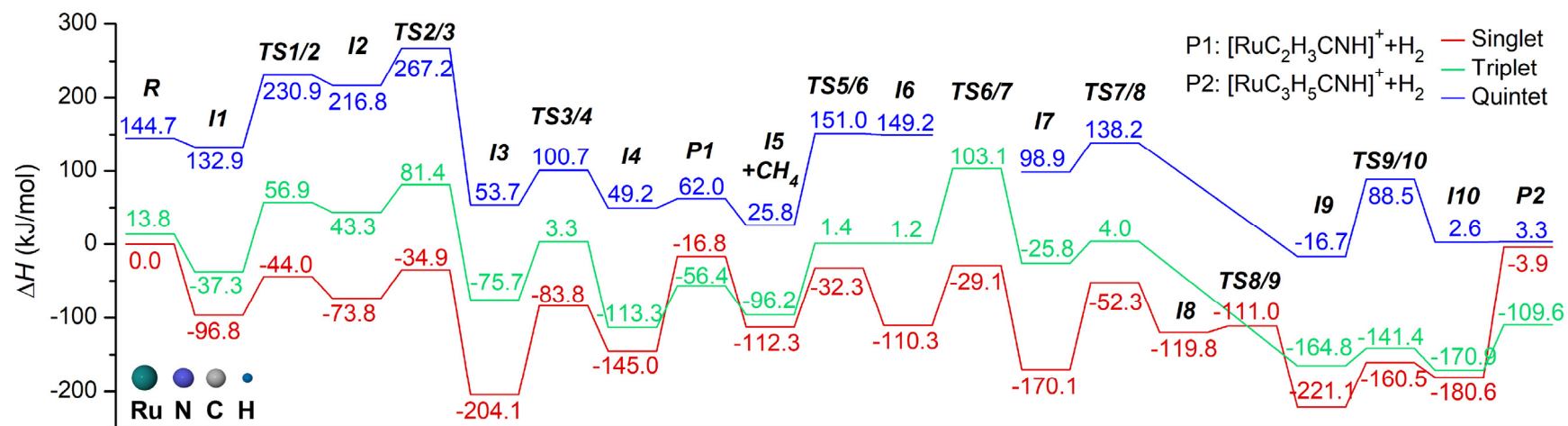


Fig. S21 PES for the reaction of $[\text{RuCHCNH}]^+$ with CH_4 toward product P1 and P2. Energies are in kJ/mol.

As shown in Fig. 2b and Fig. S21, the process of CH₄ activation by product **P1** ³[RuCHCNHCH₂]⁺ ([HNC-Ru-CH-CH₂]⁺) is similar to that of [RuCHCNH]⁺ ([HNC-Ru-CH]⁺). That is, first hydrogen transfer (**TS5/6** → **I6**), C-C bonding (**TS6/7** → **I7**), second hydrogen transfer (**TS9/10** → **I10**) occur in sequence, finally leading to the formation and desorption of H₂. Also, the charge and spin populations on the transferring hydrogen of singlet ¹**TS5/6** and ¹**TS9/10** are respectively close to 0 and 1 (Fig. S24), proving a HAT process. The only difference is that before the second round of hydrogen transfer to Ru, an alkyl isomerization process (**TS7/8** → **I8**) is needed to lay the groundwork for the generation of exothermic product **P2** [RuCHCNH(CH₂)₂]⁺ ([HNC-Ru-CH₂CHCH₂]⁺). And the direct bonding of CH₃ with CH of [RuCHCNHCH₂]⁺ ([HNC-Ru-CH-CH₂]⁺) from **I6** to **I8** (or **I9**) is relatively difficult to be achieved due to the larger energy barriers (Fig. S22, **TS6/7***), further explaining the necessity of alkyl isomerization. It should be pointed out that the relative energies of ¹**TS5/6** (-32.3 kJ/mol), ¹**TS6/7** (-29.1 kJ/mol) and ¹**TS7/8** (-52.3 kJ/mol) are higher than ³**P1** (-56.4 kJ/mol), indicating the triplet ionic product ³[RuCHCNHCH₂]⁺ with the lowest energy cannot directly dehydrogenate CH₄ at room temperature. While the spin-conserved pathway with the generation of singlet ¹**P1** (-16.8 kJ/mol, Fig. S21) is more favorable than the TSR process, thus enables the occurrence of second CH₄ activation by [RuCHCNHCH₂]⁺.

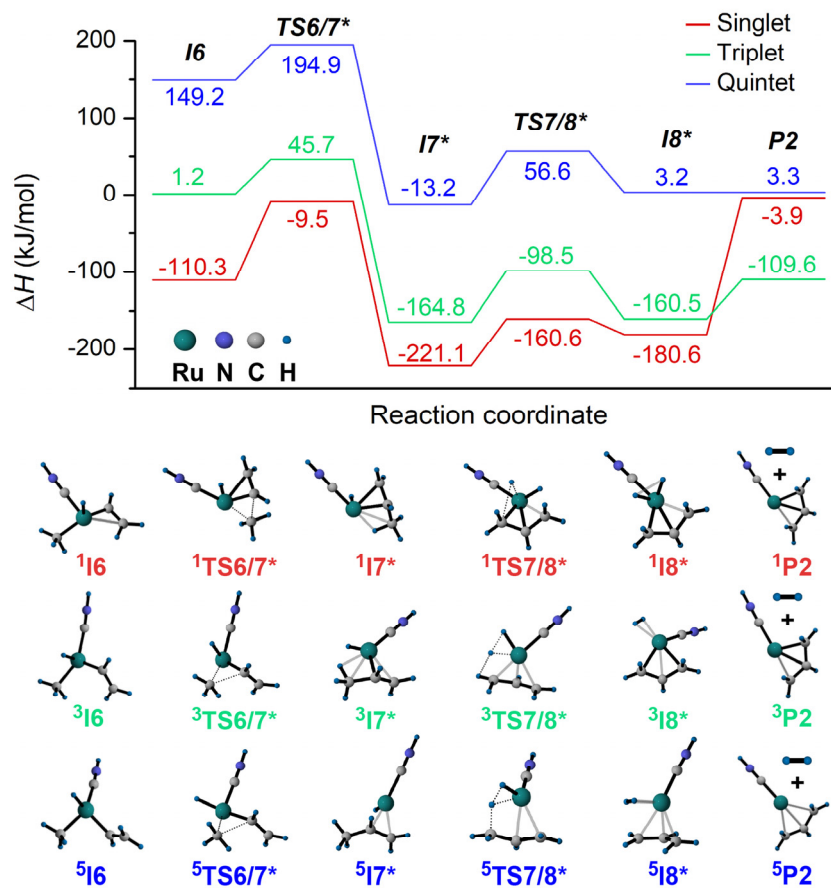


Fig. S22 PES for the reaction of $[\text{RuCHCNH}]^+$ with CH_4 toward product P_2 . Energies are in kJ/mol.

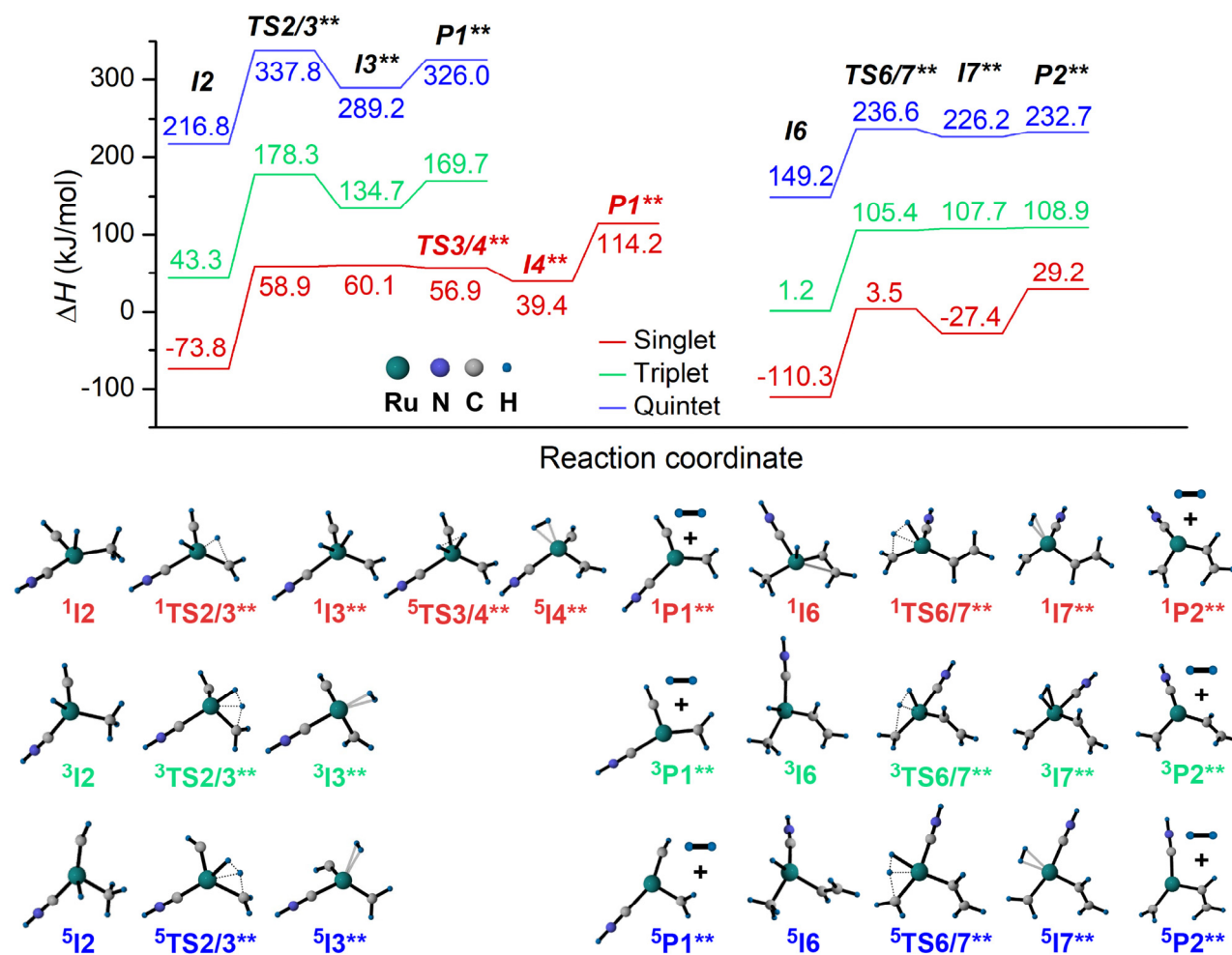


Fig. S23 PES for the reaction of $[\text{RuCHCNH}]^+$ with CH_4 toward product P^{**} . Energies are in kJ/mol.

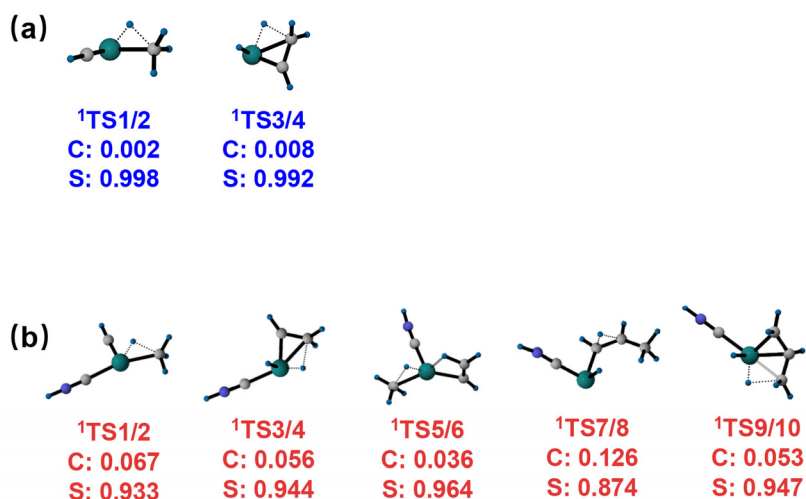


Fig. S24 Charge and spin populations on the transferring hydrogen of H involved transition states of $[\text{RuCH}]^+$ and $[\text{RuCHCNH}]^+$. Charge population and spin population are abbreviated as “C” and “S”, respectively.

(a)	$^2[\text{RuC}]^+$	$^3[\text{RuCH}]^+$	(b)	$[\text{RuC}]^+/\text{CH}_4$ 2_1	$[\text{RuCH}]^+/\text{CH}_4$ 3_1
	Ru	Ru		Ru	Ru
	s 0.00	s 0.00		s 0.01	s 0.01
	p 0.00	p 0.00		p 0.01	p 0.02
	d 100.00	d 99.99		d 99.97	d 99.87
	1.00e	1.00e		0.99e	0.99e
					1.00e
					1.00e
(c)	$[\text{RuC}]^+/\text{CH}_4$ $^2\text{TS1/2}$	$[\text{RuCH}]^+/\text{CH}_4$ $^1\text{TS1/2}$	(d)	$[\text{RuC}]^+/\text{CH}_4$ $^2\text{TS2/3}$	$[\text{RuCH}]^+/\text{CH}_4$ $^1\text{TS3/4}$
	Ru	Ru		53.8% Ru	55.35% Ru
	s 0.17	s 0.02		s 41.68	s 25.87
	p 0.14	p 0.05		p 3.54	p 1.54
	d 99.63	d 99.90		d 54.67	d 72.51
	0.92e	0.96e		46.2% H	44.65% C
				s 99.52	s 5.70
				p 0.46	p 93.97
				d 0.02	d 0.31
				0.83e	0.40e
					1.65e

Fig. 25 Composition and occupancy of alpha and beta HOMOs of (a) $[\text{RuL}]^+$ (**R**), (b) encounter complexes (**I1**) and transition states involved in the (c) first and (d) second rounds of hydrogen transfer. Red, black and blue numbers display the orbital contribution, subshell composition and electron occupancy.

The hybridized orbitals with significantly decreased electron occupancy give rise to active electron-deficient states, which could be essential for proceeding of HAT processes as mentioned above. This agrees well with the PESs results: i) HOMOs of **R** and **I1** involving $[\text{RuCH}]^+$ and $[\text{RuC}]^+$ are both dominated by d orbitals of Ru, thus resulting in inferior difference in the formation of

encounter complex. In contrast, the active involvement of s orbitals of H in transition state for $[\text{RuCH}]^+/\text{CH}_4$ provides an obvious advantage over $[\text{RuC}]^+/\text{CH}_4$ during H transfer. ii) After having formed a “H ligand” on Ru (**12**) via the first round of H transfer in $[\text{RuC}]^+/\text{CH}_4$, s and p orbitals of H and C contribute to the electron-deficient HOMOs of $[\text{RuC}]^+/\text{CH}_4$ ($[\text{H-RuC-CH}_3]^+$) in the second round of hydrogen transfer, causing significantly lower (but still hardly feasible) transition states (**TS2/3**, Fig. S13, S16). Thus, although ligand H is not directly involved in orbital formation, here it may have an effect on the composition of HOMOs which determines the accomplishment of CH_4 dehydrogenation.

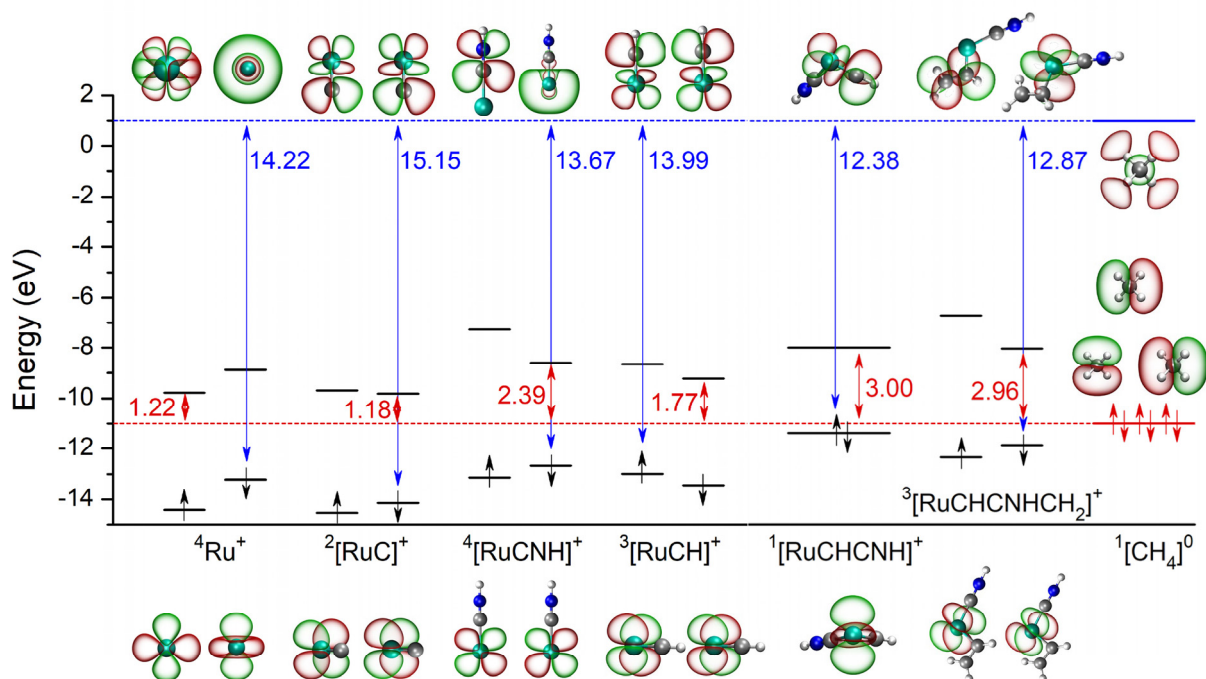


Fig. S26 HOMOs (bottom) and LUMOs (top) of $[\text{RuL}]^+$ and CH_4 .

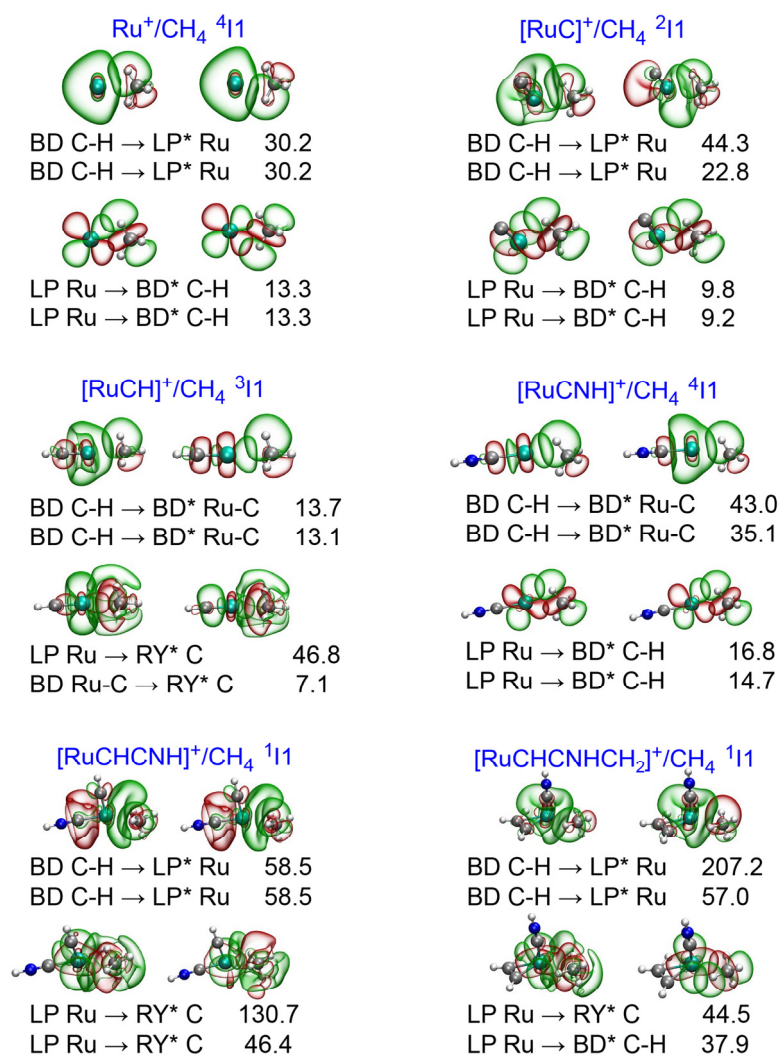


Fig. S27 Natural bond orbital (NBO) analysis of $[\text{RuL}]^+/\text{CH}_4$. Energies are in kJ/mol.

2. References

- 1 a) N. Dietl, C. van der Linde, M. Schlangen, M. K. Beyer, H. Schwarz, *Angew. Chem. Int. Ed.* **2011**, *50*, 4966-4969; b) X. N. Wu, Y. X. Zhao, W. Xue, Z. C. Wang, S. G. He, X. L. Ding, *Phys. Chem. Chem. Phys.* **2010**, *12*, 3984-3997; c) S. Feyel, J. Doebler, R. Hoeckendorf, M. K. Beyer, J. Sauer, H. Schwarz, *Angew. Chem. Int. Ed.* **2008**, *47*, 1946-1950.